Defect-induced ferromagnetism in undoped and Mn-doped zirconia thin films

Jan Zippel,[1] Michael Lorenz,[1,*] Annette Setzer,[1] Gerald Wagner,[2] Nikolai Sobolev,[3] Pablo Esquinazi,[1] and Marius Grundmann[1]

[1]*Institut für Experimentelle Physik II, Universität Leipzig, Linnéstraße 5, D-04103 Leipzig, Germany*

[2]*Institut für Mineralogie, Kristallographie und Materialwissenschaften, Universität Leipzig, Scharnhorststraße 20, D-04275 Leipzig, Germany*

[3]*Departamento de Física and I3N, Universidade de Aveiro, 3810-193 Aveiro, Portugal*

(Received 1 July 2010; revised manuscript received 20 August 2010; published 24 September 2010)

A doping-independent ferromagnetic hysteresis at 300 and 5 K was found for both undoped and Mn-doped zirconia thin films with up to 20 at. % Mn. The lack of Mn-induced magnetic ordering is a strong indication that the observed ferromagnetic effects are defect related. Electron paramagnetic resonance analysis supports the conclusion that Mn ions are in a magnetically "silent" state. Cubic ZrO_2:Mn films show a noticeable layer ferromagnetic saturation magnetization at 5 K, as compared to the monoclinic and tetragonal films, which clearly correlates with strain and a higher density of dislocations as the dominating microstructural defect.

DOI: 10.1103/PhysRevB.82.125209 PACS number(s): 75.70.−i, 75.47.Lx, 77.55.Px, 81.15.Fg

Magnetic effects in oxides have gained considerable attention in recent years due to the theoretical prediction of diluted magnetic semiconductors with high Curie temperature (T_c) and promising applications as spintronic materials.[1,2] However, the experimental search for ferromagnetism in transition-metal-doped ZnO did not result up to now in reproducible and homogeneous magnetic materials.[3–5] Sometimes clustering was found to be responsible for the observed magnetism in ZnO,[6] and also in TiO_2.[7] Later on, weak ferromagnetism was even detected in completely undoped ZnO, giving evidence that defects could be the origin of the observed effects.[8–10] Recently, models were proposed to explain the weak ferromagnetic effects in ZnO and TiO_2 as defect related.[10,11] Beside ZnO and TiO_2, also other oxides appear more and more in the focus of research with regards to their magnetic properties, as, for example, SnO_2, or In_2O_3,[1,4] and HfO_2.[12]

In this paper, we focus on zirconia (ZrO_2), which shows interesting properties such as a high dielectric constant and ionic conductivity. Recently it was predicted from density-functional theory calculations that Mn-stabilized cubic zirconia should be ferromagnetic above room temperature.[13,14] The high-T_c ferromagnetism was predicted to be robust to oxygen-vacancy defects and to the particular Mn impurity distribution in the Zr fcc sublattice.[13] Furthermore, a magnetic moment in between 3.0 and 3.7 μ_B per Mn atom was calculated for both interstitial and substitutional Mn for monoclinic, tetragonal, and cubic zirconia with 25% Mn.[14]

Initiated by these promising predictions, several experimental attempts were started to confirm experimentally the ferromagnetism in Mn-doped zirconia. However, nanocrystals with 1.39% and 4.38% Mn in zirconia were found to be purely paramagnetic at room temperature.[15] Low-temperature (2 K) measurements at high field (5 T) showed hysteresis due to an antiferromagnetic coupling between the manganese-ion magnetic moments around 3.8 μ_B/Mn and 2.8 μ_B/Mn for the diluted and the higher concentrated samples, respectively.[15] Mn- and Fe-stabilized zirconia nanoparticles with up to 35% and 40% 3*d*-element content were also found to be paramagnetic at room temperature and at 5 K.[16] Schubert *et al.* has grown Mn-stabilized zirconia thin films on yttria-stabilized zirconia (YSZ) single-crystal substrates by sputtering and found an unexpected behavior of in-plane and out-of-plane misfit, resulting in a tetragonal structure.[17] In the following, we will present the magnetic properties of undoped and Mn-doped zirconia thin films grown on YSZ substrates.

Undoped and Mn-doped zirconia thin films were grown on cubic (001) oriented YSZ substrates (size $5\times5\times0.4$ mm^3) by pulsed laser deposition (PLD) using a KrF excimer laser operating at 248 nm wavelength.[18] The heater temperature and the oxygen partial pressure $p(O_2)$ were chosen between 640 and 790 °C and $0.016-3\times10^{-4}$ mbar, respectively. However, because of the phase purity (see discussion of Fig. 1) and comparability almost all films discussed in the following were grown at 720–790 °C. The oxygen partial pressure in the above-mentioned range had little influence on the film structure and composition as will be shown elsewhere. Film thickness was between 400 and 700 nm.[19] The PLD targets were pressed and sintered from ZrO_2 powder (Fluka, purity better 99%, naturally accompanied by about 1% HfO_2) and MnO_2 powder (Alfa Aesar 99.999%). According to information from the supplier, the most prominent anion traces in zirconia powder are SiO_2, SO_4^{2-}. Common cation traces are Ti, Al, and with concentration in the 100 ppm range also Fe. However, as examined carefully in Ref. 10, Fe trace impurities from 50 to 250 ppm in ZnO films do not induce any relevant ferromagnetic signals. We investigated several film series grown from undoped and doped zirconia targets with 10 at. % and 20 at. % MnO_2. Reproducible results based on the three different source target compositions will be presented in the following.

The Mn transfer from the targets via the PLD process into the films is nearly stoichiometric in relation to zirconium, as analyzed by Rutherford backscattering spectroscopy (RBS), proton-induced x-ray emission (PIXE), and energy-dispersive x-ray spectroscopy (EDX). We found from 9 to 14 at. % and 18 to 23 at. % Mn in the films, for the targets with 10% and 20% Mn, respectively, with the growth temperature being the most important PLD parameter. The surfaces of all grown thin films appear quite smooth in atomic

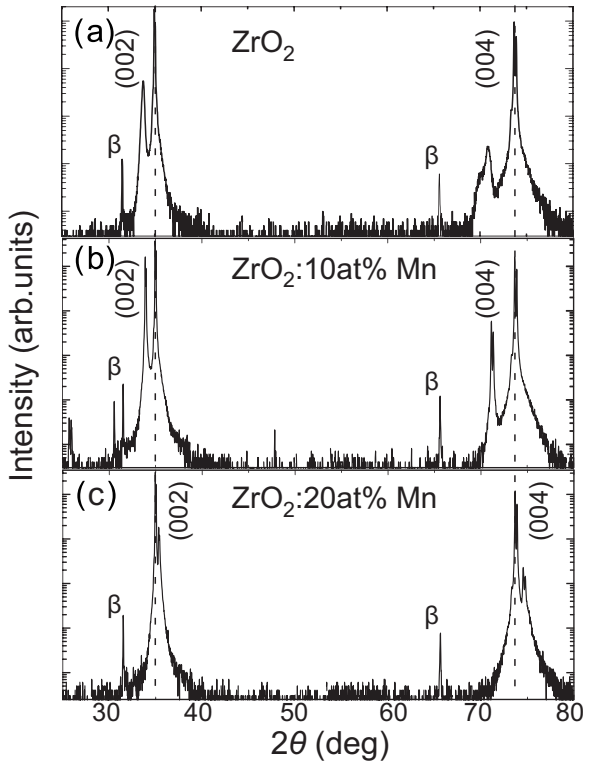

FIG. 1. XRD 2Θ-ω scans of typical ZrO_2-based films on YSZ(001) substrates. (a) Undoped ZrO_2 film in monoclinic phase, (b) doped ZrO_2 film with 10 at. % Mn in monoclinic phase, and (c) ZrO_2:20 at. % Mn film in cubic phase. The (002) and (004) reflections of the cubic YSZ substrates are indicated by the dashed lines. The position of the out-of-plane film peaks corresponds to the slightly increased (a) and (b) or decreased (c) out-of-plane lattice constant of the films. The films shown here were grown at 720–790 °C and with $p(O_2)$ of 0.002 mbar. β marks the weak spectral Cu $K\beta$ lines.

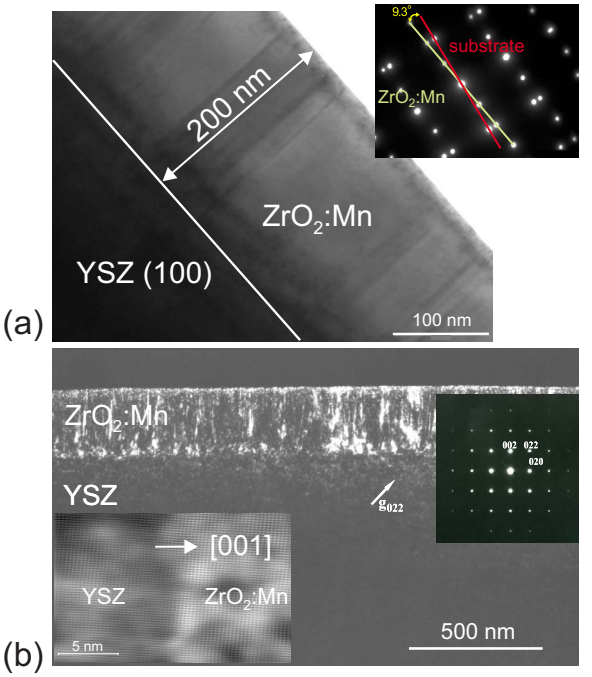

FIG. 2. (Color online) (a) Bright-field TEM image of a monoclinic ZrO_2:10%Mn film (by D. Hesse MPI Halle) and (b) TEM weak beam dark-field (100) cross section (g, 3g) of a cubic ZrO_2:20%Mn film. The cubic film (b) shows a higher density of dislocation lines as compared to the monoclinic film (a). The insets in (a) and (b) show SAD patterns of film and substrate. The SAD pattern in (a) shows clearly the rotation of YSZ and ZrO_2:Mn patterns of 9.3°, proving the monoclinic film phase. The SAD pattern in (b) reveals no deviation of substrate and film reflections, confirming the cubic film phase. The Fourier filtered HR-TEM image in (b) shows the interfacial region of the lattice matched, cubic ZrO_2:20%Mn film and the YSZ substrate.

force microscopy (AFM). The root-mean-square values of the surface roughness extracted from 1×2 μm^2 AFM scans with a Park XE-150 were in between 0.13 and 0.25 nm.

The crystalline film structure was examined by wide-angle x-ray diffraction (XRD) and high-resolution XRD (HR-XRD) measurements using a Philips X'Pert diffractometer with Cu $K\alpha$ and Cu $K\alpha1$ radiation, respectively. Figure 1 shows typical XRD 2Θ-ω scans of undoped and doped films. From the relative positions of film peaks to the fixed YSZ (002) and (004) substrate peaks in Fig. 1, we see clearly that films grown from undoped zirconia target and zirconia with 10 at. % Mn exhibit monoclinic structure. 20 at. % Mn in the target stabilizes the cubic phase of the films. By slightly reducing the growth temperature of the films to less than 730 °C, in addition to the cubic phase an additional tetragonal phase of the films was identified. As to the intermediate Mn concentration range, a partial stabilization of the cubic phase begins with 14 at. % Mn in the ZrO_2 films. From the corresponding out-of-plane peaks (Fig. 1) and the skew-symmetric (202) peaks, the following out-of-plane and in-plane lattice constants $c_{m,c,t}$ and $a_{m,c,t}$ of the three different phases were determined. We obtained a_m=5.304 to 5.307 Å, c_m=5.142 to 5.146 Å, and a_c=c_c=5.06 to 5.09 Å, and a_t=5.13 to 5.14 Å, c_t=5.20 to 5.11 Å, for the monoclinic, cubic, and tetragonal phase, respectively. The given ranges of lattice constants are due to the above-mentioned range of PLD growth conditions. Nevertheless, the obtained values are in consistent agreement with other published lattice constants for Mn-stabilized ZrO_2 thin films, see the detailed overview on structural properties in Ref. 17.

Figure 2 shows the typical crystalline microstructure of zirconia films grown from the targets with (a) 10% Mn and (b) 20% Mn. In agreement with the x-ray analysis (Fig. 1), 10% Mn results in the monoclinic phase, as proved by the selected area diffraction (SAD) image in Fig. 2(a), which shows the monoclinic angle of ZrO_2 of 99.3°.[17] Although the films are grown on a nearly homoepitaxial substrate, the monoclinic layers show columnar defect bands with antiphase domains and dislocations. In between these regions, the layer seems to be relatively defect free. The transmission electron microscopy (TEM) cross section of the cubic film with larger Mn content in Fig. 2(b) shows an even higher density of dislocation lines. In addition, the higher tilt mosaicity of the cubic films in comparison to the monoclinic films is quantitatively confirmed by HR-XRD rocking curve widths of the ZrO_2 (002) film and substrate reflections, see Table I. However, apart from the dislocation lines, no indi-

TABLE I. Full width at half maximum of HR-XRD rocking curves of the ZrO_2 and YSZ (002) reflections of the indicated samples. The number in parentheses is the number of different samples investigated. The rocking curves were measured as ω scan with the open detector fixed at the 2Θ position of the corresponding Bragg peak, compare the XRD wide-angle scans in Fig. 1.

Sample (samples involved)	FWHM ZrO_2(002) (arc sec)
YSZ substrates (10)	19–83
ZrO_2 film monoclinic (1)	122
ZrO_2:10%Mn films monoclinic (4)	86–94
ZrO_2:20%Mn films cubic (4)	252–660

cations for phase separation or nanocrystalline cluster segregations were found for both monoclinic and cubic zirconia films. In addition, the high-resolution TEM image in Fig. 2(b) shows on a microscopic scale a nearly identical cubic structure of both YSZ substrate and ZrO_2:Mn film, proving close in-plane lattice match of cubic zirconia on YSZ, with few mismatch dislocations.

The magnetic properties were investigated using a superconducting quantum interference device (SQUID) magnetometer (Quantum Design MPMS-7) with reciprocating sample option and a resolution of better than 10^{-7} emu. Hysteresis loops at 300 K (Fig. 3) and 5 K (Fig. 5) between ± 50 kOe as well as the temperature dependence at 1 T (Fig. 4) were measured. For all measurements, the magnetic field was applied in-plane, i.e., perpendicular to the growth direction.

The magnetic effect of the used substrates was carefully subtracted from the initial measurements to extract the remaining film signals only. The 5×5 mm^2 YSZ substrates were identical pieces cut from the same 10×10 mm^2 wafer used also for the films. Before correction, the substrate signals were normalized to equal sample mass which is typically ~40 mg. Because in general the substrate signals were less than a quarter of the film signals the results shown in Figs. 3–6 are clearly film related. To simulate the effect of

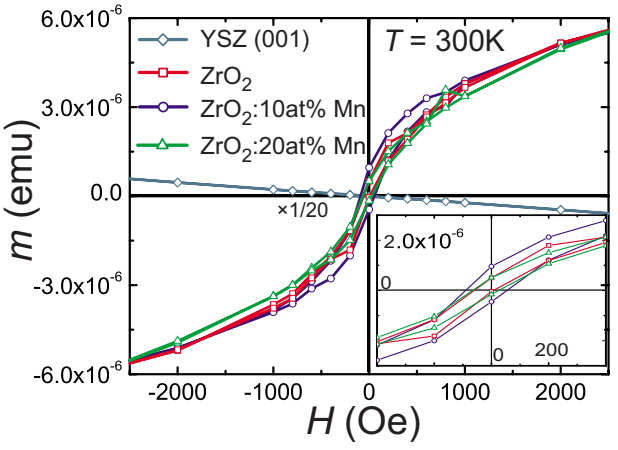

FIG. 3. (Color online) Ferromagnetic hysteresis of doped ZrO_2:Mn (with 10.4 and 21.3 at. %Mn) and undoped ZrO_2 films at 300 K, after subtraction of the substrate background. The diamagnetic $m(H)$ of a YSZ(001) substrate is divided by 20. The coercive fields of the film hysteresis are in between about 45 and 85 Oe, as demonstrated in the inset.

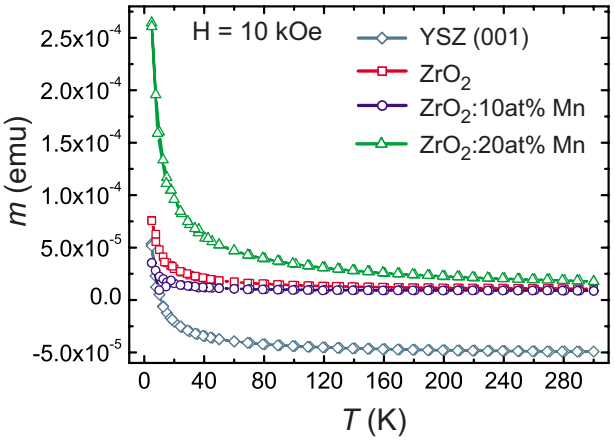

FIG. 4. (Color online) Temperature dependence of the magnetic moment at 10 kOe for a YSZ(001) substrate and undoped and doped zirconia films with 10% and 20% Mn, compare Figs. 3 and 5. For the film curves, the mainly diamagnetic YSZ substrate contribution was subtracted.

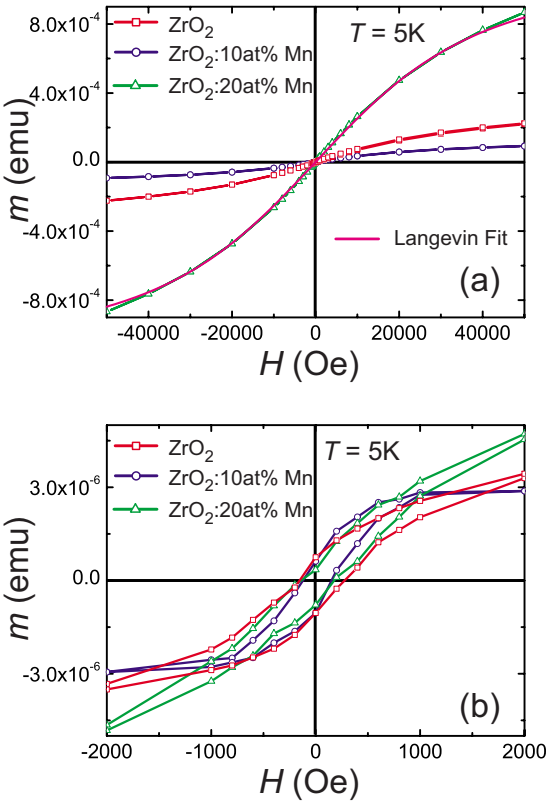

FIG. 5. (Color online) (a) Typical S-shaped m-H plots taken for ZrO_2:Mn and ZrO_2 films on YSZ at $T=5$ K. The experimental data of the cubic sample with 20% Mn were fitted with the Langevin function using $N=4.87\times10^{20}$ cm^{-3} and $\mu=4.78$ μ_B. (b) Ferromagnetic hysteresis of doped and undoped zirconia films, obtained by subtracting the paramagnetic fraction from the initial SQUID data in (a). The coercive fields are in between about 95 and 205 Oe at 5 K.

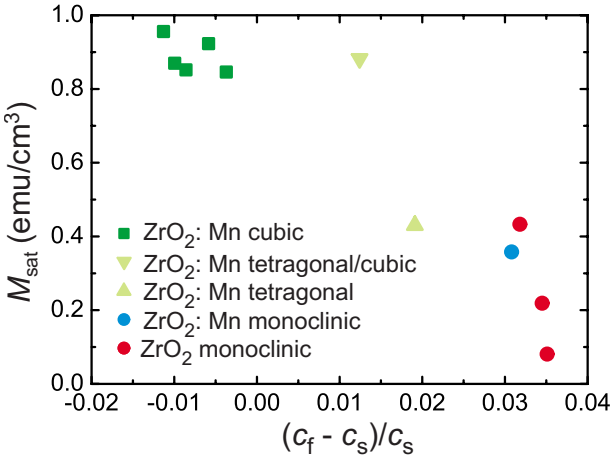

FIG. 6. (Color online) Ferromagnetic saturation magnetization M_{sat} at 5 K of all films in relation to the out-of-plane lattice strain calculated from the c-axis lattice constants c_f and c_s of film and substrate, respectively. Here, M_{sat} is normalized to the film volume. Obvious are clear correlations of M_{sat} to the crystalline phase and the corresponding out-of-plane lattice strain.

the high-temperature PLD growth on the substrate magnetization, we measured also substrates annealed in oxygen, which did not show a change in magnetization.

Figure 3 shows the magnetic moment-field (m-H) plots at 300 K for films from the three different source target compositions. An open, i.e., ferromagnetic hysteresis loop becomes visible for all films at 300 K, in particular, also for the undoped zirconia film. To understand this doping-independent behavior, one should consider that diluted Mn atoms can appear in three different magnetic states. First, the contribution from a few isolated Mn ions in the zirconia host lattice should be paramagnetic. Second, a direct coupling between nearest-neighbor Mn ions would give an antiferromagnetic contribution. Third, only Mn ions coupled via oxygen vacancies or oxygen ions (double exchange) can yield to a ferromagnetic signal. However, it remains unclear in which particular state the Mn atoms are in our samples. According to Ref. 20, it is necessary to create at least 8 mol % oxygen vacancies in order to stabilize the cubic phase in zirconia. Assuming that either one Mn^{2+} or two Mn^{3+} ions yield one oxygen vacancy, together with the mentioned fact that at least ~15 at. % Mn in the films is necessary to stabilize a tetragonal or cubic structure, leads to the conclusion that the valence state Mn^{3+} should prevail in our films. Additional support for this assumption comes from a comparison with the solid-state phase diagram of manganese oxides,[21] where the dominance of Mn^{3+}, or at least of a mixed state $Mn^{3+/2+}$, i.e., Mn_3O_4, is favored for our PLD growth conditions. Figure 4 shows the temperature dependence of the magnetic moment of doped and undoped films. The low-temperature $1/T$ dependence is a clear indication for the dominating paramagnetism, in addition to the weak ferromagnetic signal.

Electron paramagnetic resonance (EPR) experiments in the X band at 9.4 GHz at 300 K to 10 K in perpendicular and parallel magnetic field orientation did not show remarkable differences between thin films with 10 at. % and 20 at. % Mn and the pure YSZ substrate (not shown here). In addition, no angular dependence of EPR signals was observed. A possible explanation can be again that Mn is present mainly as Mn^{3+}, which is EPR silent.

At $T=5$ K, the samples reveal S-shaped m-H curves typical of a paramagnetic contribution, see Fig. 5(a). This favors the fact that the Mn ions are isolated and therefore contribute only with a paramagnetic fraction, as introduced above. The shape of the m-H plot can be well fitted by using a Langevin function, i.e., $m=N\mu\times[\coth(\mu H/k_BT)-k_BT/\mu H]$. Therein, N is the number of magnetic particles per cubic centimeter and μ represents the magnetic moment per particle. In Fig. 5(a), the fit of the m-H plot for the sample containing 21.3 at. % Mn is included. From the fit we obtain a magnetic particle density N of $\sim 4.9\times 10^{20}$ cm^{-3} and a relatively high moment μ of about 4.8 μ_B per Mn atom. A Brillouin fit leads to similar high moments. For comparison, Ref. 22 reports μ values from 4.85 to 5.9 μ_B for Mn ions in glass networks.

By assuming, that mainly Mn atoms contribute to the observed paramagnetic effect, we get for the thin film with 21.3 at. % Mn a much lower "magnetic" Mn content of only ~10%. For the thin film with 10.4 at. % Mn, the Mn content obtained from the Langevin fit is below 1 at. % and for the pure ZrO_2 thin film, the fit parameters are $N=9.5\times 10^{19}$ cm^{-3} and $\mu=5.8$ μ_B. The large discrepancies between the nominal Mn concentrations (as measured by EDX and RBS) and the paramagnetic fit values indicate that only a portion of all chemically incorporated Mn atoms are in a paramagnetically active state. At such high Mn concentrations and following random statistical arguments,[23] we may expect that much of the Mn ions could be antiferromagnetically coupled and thus not contributing to the macroscopic magnetization.

The results suggest that the paramagnetic signals could come from defects instead of Mn ions. Especially taking into account the result of the undoped film, we conclude that structural defects appear as the magnetic centers and that the particle density N and moment μ refer to the magnetically active defect centers. A defect density of 10% appears as a well accepted upper limit in thin films. By subtracting the paramagnetic contribution given by the fitted Langevin function, hysteresis loops with similar open area become visible indicating a weak ferromagnetic ordering in all samples as depicted in Fig. 5(b). For the monoclinic ZrO_2 film with 10.4% Mn, we observe the lowest saturation magnetic moment. For the cubic film with 21.3% Mn, the magnetic moment does not saturate up to 5 T.

Figure 6 shows the ferromagnetic saturation magnetization of all films as a function of the out-of-plane lattice strain. All cubic ZrO_2:Mn films show saturation magnetizations which are a factor of about 3–10 higher than that of the monoclinic films. This considerable enhancement of the saturation magnetization rules out that the ferromagnetic hysteresis is induced mainly by the chemical Mn content or possible trace impurities in the zirconia source target material. Instead, structural effects appear as possible origin of the differences of magnetic performance as discussed above. As well known in ZnO and TiO_2, defects, especially vacancies could be responsible for the observed ferromagnetic behavior.[10,11,24,25] Whether the ferromagnetic be-

havior observed is intrinsic due to a real ferromagnetic state or to a diluted antiferromagnetic state in an applied magnetic field, which may show similar weak hysteresis loops,[26] has to be clarified in future studies, especially by measuring the temperature dependence of the magnetization near the ordering critical temperature at different applied fields.

A comparison of the TEM images in Fig. 2 and of the (002) rocking curve widths in Table I of the monoclinic and cubic ZrO_2:Mn films indicates a higher dislocation density in the cubic films, in correlation with the increased magnetization in Fig. 6. Obviously, the monoclinic structure is a more relaxed structure with more possibility of strain compensation instead of the development of structural defects in the cubic structure. The obvious dependence of M_{sat} to the out-of-plane strain state of the films (Fig. 6) is a clear evidence for the structural dependence of the ferromagnetic saturation magnetization. The magnetization is highest for reduced out-of-plane lattice constant, corresponding to tensile in-plane strain. However, the particular nature of the magnetic defects and the question of possible defect accumulation at the film surface or interface are tasks for further investigations of zirconia thin films.

We thank Dietrich Hesse, MPI Microstructure Physics Halle, for the TEM image in Fig. 2(a) and for fruitful discussions. We are indebted to G. Ramm, H. Hochmuth, C. Meinecke, S. Schöche, T. Böntgen, H. Hilmer, Amélia O. Ankiewicz, and Nuno M. Santos for growth of the films by PLD, RBS/PIXE analysis, spectroscopic ellipsometry, and EPR investigations, respectively. Financial support of the Deutsche Forschungsgemeinschaft within the SFB 762 "Functionality of oxide interfaces," of the European Social Fund (ESF), and the Leipzig School of Natural Sciences BuildMoNa (GS 185), and of the Portuguese-German collaboration project Acção Integrada (Project No. A-17/10), and of the FCT of Portugal (Project No. PTDC/FIS/72843/2006) is kindly acknowledged.

*Author to whom correspondence should be addressed; mlorenz@physik.uni-leipzig.de

[1] W. Prellier, A. Fouchet, and B. Mercey, J. Phys.: Condens. Matter **15**, R1583 (2003).
[2] M. Venkatesan, C. B. Fitzgerald, J. G. Lunney, and J. M. D. Coey, Phys. Rev. Lett. **93**, 177206 (2004).
[3] Z. Jin, T. Fukumara, M. Kawasaki, K. Ando, H. Saito, T. Sekiguchi, Y. Z. Yoo, M. Murakami, Y. Matsumoto, T. Hasegawa, and H. Koinuma, Appl. Phys. Lett. **78**, 3824 (2001).
[4] T. Fukumura, H. Toyosaki, and Y. Yamada, Semicond. Sci. Technol. **20**, S103 (2005).
[5] M. Ungureanu, H. Schmidt, H. von Wenckstern, H. Hochmuth, M. Lorenz, M. Grundmann, M. Fecioru-Morariu, and G. Güntherodt, Thin Solid Films **515**, 8761 (2007).
[6] A. Ney, M. Opel, T. C. Kaspar, V. Ney, S. Ye, K. Ollefs, T. Kammermeier, S. Bauer, K.-W. Nielsen, S. T. B. Goennenwein, M. H. Engelhard, S. Zhou, K. Potzger, J. Simon, W. Mader, S. M. Heald, J. C. Cezar, F. Wilhelm, A. Rogalev, R. Gross, and S. A. Chambers, New J. Phys. **12**, 013020 (2010).
[7] S. Zhou, K. Potzger, G. Talut, A. Shalimov, J. Grenzer, W. Skorupa, M. Helm, J. Fassbender, E. Cizmar, S. A. Zvyagin, and J. Wosnitza, J. Appl. Phys. **103**, 083907 (2008).
[8] Q. Xu, H. Schmidt, L. Hartmann, H. Hochmuth, M. Lorenz, A. Setzer, P. Esquinazi, C. Meinecke, and M. Grundmann, Appl. Phys. Lett. **91**, 092503 (2007).
[9] Q. Xu, H. Schmidt, S. Zhou, K. Potzger, M. Helm, H. Hochmuth, M. Lorenz, A. Setzer, P. Esquinazi, C. Meinecke, and M. Grundmann, Appl. Phys. Lett. **92**, 082508 (2008).
[10] M. Khalid, M. Ziese, A. Setzer, P. Esquinazi, M. Lorenz, H. Hochmuth, M. Grundmann, D. Spemann, T. Butz, G. Brauer, W. Anwand, G. Fischer, W. A. Adeagbo, W. Hergert, and A. Ernst, Phys. Rev. B **80**, 035331 (2009).
[11] J. M. D. Coey, P. Stamenov, R. D. Gunning, M. Venkatesan, and K. Paul, New J. Phys. **12**, 053025 (2010).
[12] S. Kuroda, N. Nishizawa, K. Takita, M. Mitome, Y. Bando, K. Osuch, and T. Dietl, Nature Mater. **6**, 440 (2007).
[13] S. Ostanin, A. Ernst, L. M. Sandratskii, P. Bruno, M. Dane, I. D. Hughes, J. B. Staunton, W. Hergert, I. Mertig, and J. Kudrnovsky, Phys. Rev. Lett. **98**, 016101 (2007).
[14] X. Jia, W. Yang, M. Qin, and J. Li, J. Magn. Magn. Mater. **321**, 2354 (2009).
[15] G. Clavel, M.-G. Willinger, D. Zitoun, and N. Pinna, Eur. J. Inorg. Chem. **2008**, 863 (2008).
[16] J. Yu, L. Duan, Y. Wang, and G. Rao, Physica B **403**, 4264 (2008).
[17] M. Schubert, S. Senz, and D. Hesse, Thin Solid Films **517**, 5676 (2009).
[18] M. Lorenz, in *Transparent Conductive Zinc Oxide: Basics and Applications in Thin Film Solar Cells*, Springer Series in Materials Science Vol. 104, edited by K. Ellmer, A. Klein, and B. Rech (Springer, Berlin, 2008), Chap. 7, pp. 303–358.
[19] R. Schmidt, B. Rheinländer, M. Schubert, D. Spemann, T. Butz, J. Lenzner, E. M. Kaidashev, M. Lorenz, and M. Grundmann, Appl. Phys. Lett. **82**, 2260 (2003).
[20] X. J. Huang and W. Weppner, J. Chem. Soc., Faraday Trans. **92**, 2173 (1996).
[21] S. Isber, E. Majdalani, M. Tabbal, T. Christidis, K. Zahraman, and B. Nsouli, Thin Solid Films **517**, 1592 (2009).
[22] M. S. Reddy, G. Murali Krishna, and N. Veeraiah, J. Phys. Chem. Solids **67**, 789 (2006).
[23] T. C. Droubay, T. C. Kaspar, B. P. Kaspar, and S. A. Chambers, Phys. Rev. B **79**, 075324 (2009).
[24] S. A. Chambers, Surf. Sci. Rep. **61**, 345 (2006).
[25] B. B. Straumal, A. A. Mazilkin, S. G. Protasova, A. A. Myatiev, P. B. Straumal, G. Schütz, P. A. van Aken, E. Goering, and B. Baretzky, Phys. Rev. B **79**, 205206 (2009).
[26] U. Nowak and K. D. Usadel, Phys. Rev. B **44**, 7426 (1991).